JOURNAL OF AIRCRAFT
Vol. 32, No. 5, September–October 1995

Vortex-in-Cell Analysis of Wing Wake Roll-Up

Renato S. Ribeiro*
Empresa Brasileira de Aeronáutica, São José dos Campos, SP 12227-901, Brazil
and
Ilan Kroo†
Stanford University, Stanford, California 94305

A vortex-in-cell (VIC) method was coupled with a wing vortex-lattice model to compute steady-state wake roll-up. The vorticity concentrated on the wing and wake vortex segments is distributed to a Cartesian grid through the application of a spreading function. A subvortex technique is introduced to refine the wake description without altering the number of wing panels. The velocity field induced by the spread vorticity is computed using an infinite domain fast Poisson solver. Interpolation provides velocities at any point inside the grid. The VIC method is used to compute velocities for a wake relaxation procedure and to correct wing panel circulations. The iterative method developed can be applied to configurations with several wings. The method was tested for various one- and two-wing problems and compared with results from experiments and from other theories with very good agreement. Detailed descriptions for wake geometry and accurate load distributions were obtained, even for cases where wakes intercepted wings directly.

Nomenclature

$[AIC]$	=	influence coefficient matrix
AR	=	aspect ratio
$\{BC\}$	=	boundary condition vector
b	=	wingspan (of generating wing)
C_L	=	lift coefficient
C_l	=	section lift coefficient
C_N	=	normal force coefficient
C_n	=	section normal force coefficient
C_p	=	pressure coefficient
c	=	wing local chord
c_{avg}	=	mean geometric chord
c_f	=	chord of following wing
c_g	=	chord of generating wing
M	=	total number of grid cells
M'	=	maximum number of cells at boundary planes
NI, NJ, NK	=	last grid-cell indices for x, y, and z
N_{sub}	=	number of subvortex divisions
$\boldsymbol{U}_\infty$	=	freestream velocity
$\boldsymbol{u}$	=	flow velocity
X_{cutoff}	=	position of $i = NI$ grid plane
x, y, z	=	Cartesian coordinate system
z_v	=	vertical position of following wing, relative to generating wing vortex
α	=	angle of attack
$\{\Gamma\}$	=	wing panel circulation vector
$\Delta x, \Delta y, \Delta z$	=	grid-cell dimensions
$\tilde{\phi}$	=	three-dimensional spreading function
ϕ_x, ϕ_y, ϕ_z	=	one-dimensional quadratic splines
$\boldsymbol{\psi}$	=	vector potential for velocity
$\boldsymbol{\omega}$	=	vorticity

Received April 5, 1993; revision received Nov. 18, 1994; accepted for publication Feb. 21, 1995.

*Computational Aerodynamics Engineer; currently Applications Engineer, Cray Research do Brasil, Av. Roque Petroni Jr., 999/13, São Paulo, SP 04707-910, Brazil. Member AIAA.

†Associate Professor, Department of Aeronautics and Astronautics. Member AIAA.

Introduction

THE problem of the interaction between vortex wakes and wings is very common in aircraft analysis and design. Several aerodynamic computations require the accurate description of the geometry and strength of wing wakes. Examples include wing-vortex interaction due to short interval airport takeoff, canard-wing interference, rotor analysis, and propeller-wing interference.

A rapid computational approach that provides an accurate description of vortex wakes while allowing close interactions with lifting surfaces would be a useful design tool.

Vortex-lattice and panel methods are often used in preliminary design, providing fast solutions with discretizations that involve only surface panels. These have been adapted to handle flexible wakes,[1,2] but high induced velocities sometimes create instabilities that limit the resolution of the wake or surface geometry.

The vortex-in-cell (VIC) method uses singularities to describe vorticity distributions, but their induced velocities are computed through finite difference solution of a Poisson equation. A vorticity spreading procedure, coupled with velocity interpolation, removes infinite values and smoothes the velocity field. The grid used for the Poisson solution is rectangular and requires no geometry fitting. This method had its origin in two-dimensional wake computations.[3,4] It was later extended to three dimensions[5,6] and applied to problems involving free shear layers and vortex-ring dynamics, simulating turbulent mixing processes.

The present work applies the VIC method to the wing wake roll-up problem, trying to combine the efficiency of the vortex-lattice method for wings with the robustness of the VIC formulation. It describes improvements on a method presented earlier,[7] allowing the use of finer discretizations. Several test cases are presented, for single wings and for wake-wing interactions. Results are compared with experiments and other methods.

Basic Equations and Numerical Model

Consider a system composed of one or more wings, stationary relative to each other, in low-subsonic, steady flow. A Cartesian system of coordinates is fixed to one of the wings, with the x axis in the direction of $\boldsymbol{U}_\infty$.

In the incompressible flow limit, mass continuity yields a kinematic condition to be obeyed by the flow: the velocity

field $\boldsymbol{u}$ must be divergence-free. The governing equations are linear, and allow the construction of a solution through the superposition of fundamental, singular solutions.

A vortex-lattice model uses vortex segments as building blocks. Under small perturbation conditions, wings can be modeled by their mean surfaces. The lifting surfaces thus created are covered with trapezoidal vortex rings. Steady wakes emanating from separated edges are represented by vortex lines, formed by successions of straight vortex segments.

For incompressible flows, the Kelvin–Helmholtz theorems for vortex dynamics[8] apply. Total vorticity must be conserved, either by enforcing the conservation of circulation in the flow or by assuring that the vorticity field, $\boldsymbol{\omega} = \nabla \times \boldsymbol{u}$, is also divergence-free:

$$\nabla \cdot \boldsymbol{\omega} = 0 \tag{1}$$

In addition, free vortices should move with the local fluid velocity, so as to remain force-free. Bound vortices on the wing are subjected to forces created by the fluid motion.

Velocities for an incompressible flow can be obtained by the vorticity distribution. A divergence-free velocity field is created by making $\boldsymbol{u} = \nabla \times \boldsymbol{\psi}$, defining the vector potential, $\boldsymbol{\psi}$. On the other hand, vector potential and vorticity are related by[8]

$$\nabla^2 \boldsymbol{\psi} = -\boldsymbol{\omega} \tag{2}$$

This relation yields three Poisson equations, one for each of the vector potential components, with forcing terms given by the vorticity components.

Vortex-in-Cell Method

Figure 1 presents a schematic of the VIC grid placed over the wing and wake vortices (see also Fig. 3). The x position of the last grid plane, $i = NI$, is denoted by X_{cutoff}. The boundaries of the grid box are positioned so that they are at least two grid-cells away from the vortex segments. The exception is the downstream boundary, which is crossed by the wake. Downstream of this boundary, it is assumed that the wake preserves its shape [i.e., its projection in the (yz) plane remains the same], and is aligned with the freestream direction. The influence of a portion of this "downstream wake" is taken into account by the fast Poisson solution, as explained later.

The VIC method is composed of three basic steps. First, a discrete description of the vorticity field over a regular mesh is obtained. The next step involves the discretization of the differential equation relating velocity (or vector potential) and vorticity, and solution for $\boldsymbol{u}$ at the mesh points. Finally, values

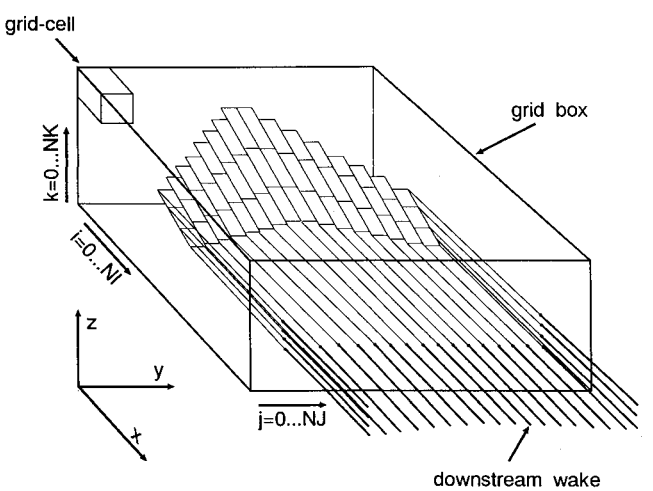

Fig. 1 Wing and wake vortices inside VIC computational grid box.

for any point inside the grid can be computed by interpolation. The method used here is based on that of Coüet.[5,6] It is essentially the same as in Ref. 7 and is described in detail in Ref. 9.

A spreading procedure provides the discrete vorticity representation in the rectangular grid. In a finite volume fashion, the vorticity $\boldsymbol{\omega}_{ijk}$ represents an average of the vorticity contained inside a grid cell. A three-dimensional spreading function $\bar{\phi}(\boldsymbol{r})$ is applied to the concentrated vorticity along the length of the vortex segments. This generates a line integral for each segment, which can be approximated by Gauss–Legendre quadratures. The spread vorticity field created by the vortex segment of extremities A and B and circulation Γ is given by

$$\boldsymbol{\omega}_{AB}(P) = \frac{\Gamma}{2} \boldsymbol{AB} \sum_{m=1}^{n} w_m \bar{\phi}(\boldsymbol{P_mP}) \tag{3}$$

n is the number of quadrature points P_m used, and w_m is a set of dimensionless weights. $\bar{\phi}$ is assembled using three one-dimensional spreading functions, so that

$$\bar{\phi}(\boldsymbol{P_mP}) = \phi_x(x - x_m) \cdot \phi_y(y - y_m) \cdot \phi_z(z - z_m) \tag{4}$$

These component functions are quadratic splines based on the grid size in their direction, and each spans three cell lengths.

The spreading function is applied to the quadrature points at each vortex segment, and $\boldsymbol{\omega}_{AB}$ is evaluated at the centers of the neighboring grid cells. This fraction of the segment vorticity is added to the previous content of the cell. In general, each point spreads to 27 cells (3 in each direction). If the vortex does not span more than one or two grid cells, two point quadratures are usually sufficient. The spreading procedure has the important property of conserving total vorticity.

In addition to the vortex segments inside the grid, the spreading procedure should be applied to two vortex segments (of length Δx) of the downstream wake.[7,9] This guarantees that the vorticity in plane $i = NI$ represents correctly the cross section of line vortices extending to $x \to \infty$.

The next step is the solution of the three Poisson equations for vector potential components, to obtain values at the grid-cell centers. This is done using a fast Poisson solver. Since perturbations should vanish far from the wing-wake system, an infinite domain solver must be employed. The algorithm used here is an adaptation of the method by James.[10] Each Poisson equation can be viewed as relating the divergence of a scalar potential (i.e., a vector potential component) to a distribution of sources (a vorticity component distribution). The scalar potential is divided into an interior and a screening potential. The problem for the interior potential contains the vorticity inside the grid and has Dirichlet boundary conditions. It is solved by the application of fast sine transforms. The operation count is of the order $(k_1 M + k_2 M \log_2 M)$, where M is the total number of grid cells. The screening potential is given by a hollow distribution of specially constructed sources or charges, and can be solved efficiently through a convolution procedure. The charges, which exist only at the boundary planes, are functions of the values for the interior potential. A solution for the potential of a single source is used in a sweep through the mesh, after manipulation of the boundary charges by two-dimensional fast sine and cosine transforms. The screening potential is finally obtained in triple-sine transformed form and added to the interior potential before the final back-transformation. The operation count for the convolution procedure is $\mathcal{O}(k_3 M + k_4 M' + k_5 M' \log_2 m')$, where M' is the maximum number of cells on the boundary planes.

An artifice was added to this method to take into account the influence of a portion of the wake downstream of the grid box. Another convolution potential is created by superim-

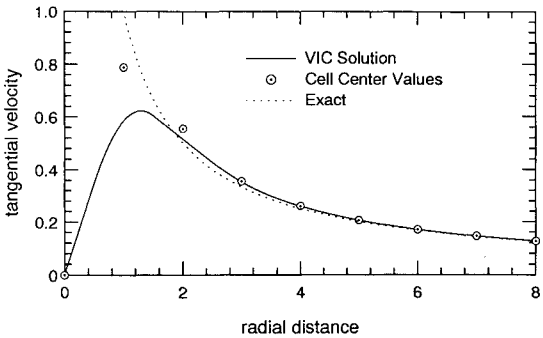

Fig. 2 Tangential velocity along a radial direction for an infinite vortex with circulation equal to 2π.

posing the influences of a line of sources on x, from plane $i = NI$ to $2NI$. When convolution with this potential is applied to the vorticity at plane NI, the effect is that of adding the influence of a wake of length $NI\Delta x$ going downstream. The crossflow shape of this wake is constant and is the shape at $i = NI$.

After the values for vector potential are known, velocities are computed by central, second-order differences.

The velocity at any point inside the grid can be determined by interpolation. The same function used for spreading is applied for interpolating the values $\boldsymbol{u}_c$ at the cell centers. The velocity at any point $P = (x, y, z)$ is given by

$$\boldsymbol{u}(P) = \sum_c \tilde{\phi}(\boldsymbol{PP}_c) \cdot \Delta x \Delta y \Delta z \cdot \boldsymbol{u}_c \tag{5}$$

where the summation occurs for the 27 cells closest to P.

The spreading/interpolation combination introduces implicitly a finite core for the vortex velocity field.[7] This effective core has a diameter (defined where velocity is maximum) of about three grid-cell lengths (see Fig. 2). Notice that, close to the core region, the interpolation does not recover the value $\boldsymbol{u}_c$ at the cell centers.

Wake Relaxation

The extremities of the vortex segments forming the wakes, referred to as nodes, are constrained to remain in $x = \text{const}$ crossflow planes. When possible, these are chosen as the same i planes that contain the grid-cell centers, so that the segment length in the x direction is Δx. The relaxation procedure is analogous to unsteady calculations of wake evolution.[11] After the determination of the velocity field by the VIC method, the velocities at all vortex nodes are computed. Then, nodes at plane i are moved in the direction of their local velocity, and the local time step is chosen so as to make them stop at plane $i + 1$. Consider a wake vortex line. If the velocity at node i is $\boldsymbol{u}_i$ and $\Delta r_x = (r_x)_{i+1} - (r_x)_i$, then

$$\boldsymbol{r}_{i+1}^{t+1} = \boldsymbol{r}_i^t + \Delta t_i \boldsymbol{u}_i \tag{6}$$

$$\Delta t_i = \Delta r_x / (u_x)_i \tag{7}$$

where t indicates the present wake geometry and $t + 1$ its next shape. $\boldsymbol{r}_i$ is the position of a node on plane i. Notice that Δr_x is equal to Δx for most segments. This process is applied simultaneously to all wake nodes. Convergence is achieved when the maximum displacement among all the nodes falls below a certain value.

Vortex-Lattice Model

In the current implementation, the vortex arrangement for the lifting surfaces is based on a model by Truckenbrodt[12] (see Fig. 3). Each wing element is trapezoidal, and is divided into N_{span} by N_{chord} panels. These are rectangular, and have the same dimensions for each chordwise row.

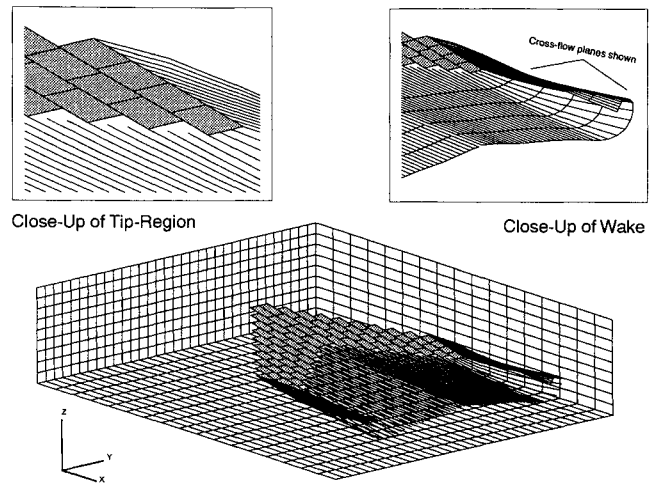

Fig. 3 Wing panel and wake vortex geometries for a swept-back wing.

Force evaluation is performed by determining C_p at the center of each panel and integrating. Therefore, only the normal component of the wing force is computed.

The Kutta condition is enforced by specifying zero circulation at the lattice trailing edges. Hence, the panels at this position must have their trailing-edge segment of vorticity canceled. This process determines the strength of the wake vortices by conserving the total circulation. Side separation can occur also, and in this case the side edge of the tip panels must have their circulation canceled.

In order to allow fine wake discretizations without increasing the number of panels, a subvortex technique was introduced.[13] Refer to the close-up in Fig. 3. At first, all wake vortices originate at wing panel corners, and their strength is determined by the Kutta condition. Then, the wake "strip" between each pair of vortices is divided into N_{sub} equal parts, creating $N_{\text{sub}} - 1$ subvortices. However, the new vortices take their circulation from the original set, so that the circulation for each original vortex is divided by N_{sub}. The strength of the new vortices is linearly interpolated from the corrected values for the original set. This refinement creates vortices that violate the Kelvin–Helmholtz theorems by starting inside the flow. The process is acceptable because these vortices are used only as markers for the wake in the VIC method.

Solution Algorithm

After the wakes are relaxed, their new geometries invalidate the boundary conditions in the wings, and the vortex-lattice problem has to be solved again. This is done by assembling the AIC matrix for the wing circulations with the influence only of the wing panels. The influence of the wake vortices on the control points is computed with the VIC method and placed as an additional boundary condition vector. The strengths Γ for the panels are then given by

$$[AIC_{\text{wings-only}}]\{\Gamma\} = -\{BC_\infty\} - \{BC^{\text{VIC}}_{\text{wakes-on-wings}}\}$$

where the first BC vector includes normal velocities on panel control points created by $\boldsymbol{U}_\infty$, and the second includes normal velocities created by the wake. This generates an iterative procedure for wing circulation correction, which can be coupled with the relaxation process. The wing panel circulations are considered converged when the maximum variation is smaller than a certain fraction of the maximum panel strength.

Therefore, after the establishment of a starting solution, the convergence loop for the algorithm has two basic steps:

1) The wing circulation is corrected by computing wake velocities using the VIC method only for the wake vorticity.

2) The wake is relaxed using velocities computed with the VIC method for all vorticity.

Results

Wake roll-up computations for a single wing aided in the study of discretization issues. Problems with close interaction between wakes and wings were studied next to evaluate the adequacy of the method for such cases. Unless otherwise stated, lengths were made nondimensional relative to the wing chord (for multiple wing arrangements, the wing of greater area was chosen).

Single Wing Analysis

The method seems to perform best when a basic guideline concerning the VIC method is followed. The discretization for the wake should place at least one vortex (preferably several vortices) per grid cell along its surface. Wing discretization should make the panel dimensions close to those of the grid cells. As in the case of wakes, at least one panel should exist per grid cell along the lifting surface. This requirement is even more important when the subvortex technique is used.

A large number of wake vortices does not compromise computational time, since this is controlled by the grid size. On the other hand, a large number of panels creates a large AIC, and may create variable storage problems. Although this matrix is decomposed only once, the time necessary may be equal to that of several VIC computations. Hence, it is convenient to keep the number of panels low, which makes their dimension comparable to that of the grid cell.

Figure 4a shows a crossflow-plane shape of the wake of an AR = 1 rectangular wing at high angle of attack. The grid used had cell dimensions equal to 0.035 × 0.035 × 0.035, and the $i = NI$ grid plane was at $x = 1.5$, measured from the leading edge. The wing had 30 × 30 panels, $N_{sub} = 10$, and side-edge separation was modeled. Notice that two turns of the tip spiral were obtained without vortex scattering. The "hook" in the roll-up center is typical of the presence of vortices with a viscous-like core.[14] Figure 4b shows the wake shape obtained when Δy and Δz were halved, without changing Δx. The wing panel length in the y direction was also halved. Small-scale instabilities appeared along the wake, indicating that the performance of the relaxation scheme was affected. The relaxation process is a time-like integration, with step size controlled by the wake segment length, which is equal to Δx. As the discretization in the (yz) plane is increased, the cell size in the x direction may need to be decreased in order to maintain the accuracy of the "time" evolution process.

Figure 5 shows normal force results for the first discretization, compared with experimental data.[15] Also shown are

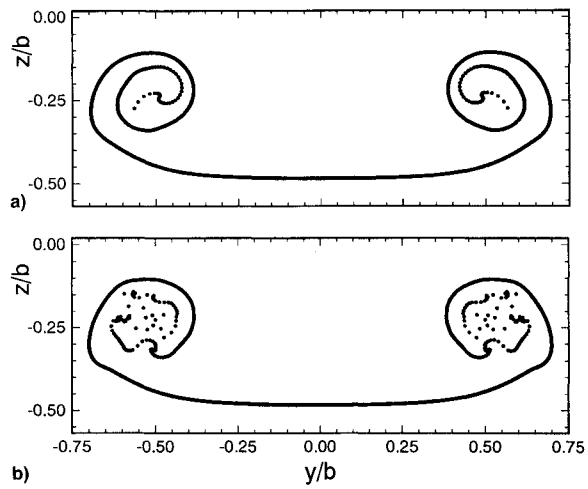

Fig. 4 Wake shape at $x = 1.5c$ for an AR = 1 rectangular wing at $\alpha = 19.4$ deg, computed with: a) 0.035 × 0.035 × 0.035 and b) 0.035 × 0.0175 × 0.0175 grid cells.

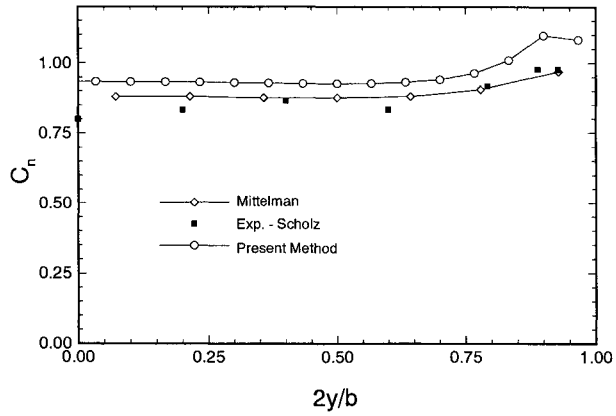

Fig. 5 Normal force distribution for AR = 1 rectangular wing at α = 19.4 deg. Present method results compared with those of Mittelman[11] and experiment.[15]

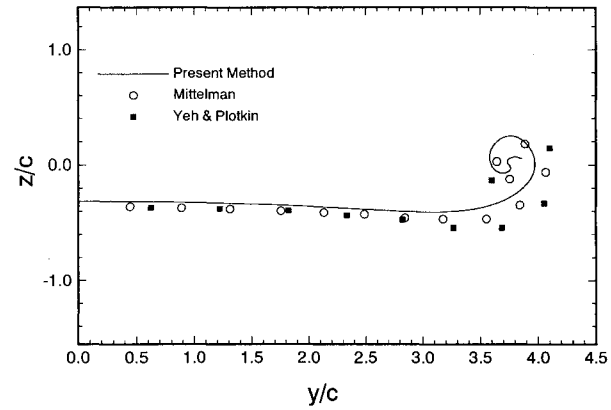

Fig. 6 Wake shape at plane $x = 5.0c$ for a rectangular wing of AR = 8 at $\alpha = 10$ deg. Comparison with results from Mittelman[11] and Yeh and Plotkin.[16]

values from a time-accurate wake roll-up method.[11] That method also used a wing vortex lattice and wake vortex segments, but displaced the wake using Biot–Savart law calculations. Agreement is good, although the present method showed a tendency to overestimate the normal force throughout the span. This is due to two factors. First, the subvortex creation tends to decrease the wake downwash on the wing control points, causing higher values for the wing panel circulations. The other factor relates to the proximity of side-edge wakes to wing panels. The wake influence on the control points is decreased because of the smoothing of the velocity field by the VIC method. This causes an increase in the wing-tip loads and affects the span loading as well.

Wake roll-up for an AR = 8 rectangular wing is shown in Fig. 6, compared again with results from Ref. 11. The values from Ref. 16 were computed using a lifting-line model for the wing and panels with linear distribution of vorticity on the wake. Notice that the present computations used a much larger number of vortices: there were 100 × 2 panels in the wing (with no side-edge wake), with $N_{sub} = 8$, amounting to 400 vortices per semispan. The grid-cell size was 0.25 × 0.075 × 0.075, with $X_{cutoff} = 14$. The origin for x is at the wing trailing edge. The VIC calculations provided a tighter roll-up, and placed the tip vorticity slightly higher.

This case was also solved using a conventional vortex-lattice roll-up method, in order to compare computational times. This was a previous version of the present code, which computed velocities using Biot–Savart law and introduced an exponential vortex-core model for each wake vortex segment. For steady-state wakes, the roll-up process can be accelerated, as explained by Maskew[1] and Katz.[2] Instead of moving all

wake nodes simultaneously, one computes the displacements for one crossflow plane and applies the same values for the remaining planes in the downstream direction. One relaxation iteration is completed when this is done for all planes, starting with the first plane upstream. After the first iteration, the wake already presents a large degree of roll-up, so that fewer velocity computations are necessary to achieve a converged wake. This acceleration technique is easy to implement when velocities are computed using Biot–Savart law summation, but is not useful for the VIC method: since velocities are obtained everywhere by the fast Poisson solver, it is better just to move all wake segments at once.

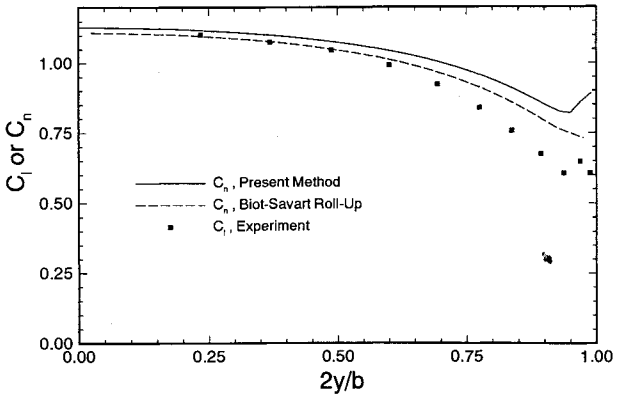

Fig. 7 Section normal force and lift distributions for a rectangular wing, AR = 6.6, α = 12.44 deg. Experimental results are from McAlister and Takahashi.[17]

Both methods used 200 × 2 panels on the wing and 200 vortices along the wake span. The rest of the parameters were the same as described previously. The computational time for the conventional method was 2.51 h in an IBM RS-6000/340 workstation. However, only 2 circulation corrections and 4 wake relaxations (with the acceleration technique described) were necessary to achieve convergence, as opposed to 6 and 113, respectively, for the VIC method. The VIC computation required 1.52 CPU hours. This indicates how the present VIC implementation provides faster velocity computations, which is important for wakes with large numbers of vortices. For nonsteady wakes, where the acceleration technique cannot be employed, the VIC method should present even greater time savings.

Figure 7 contains the section normal force distribution for a rectangular wing of AR = 6.6 at α = 12.44 deg. The VIC method used a 0.1 × 0.066 × 0.066 cell for a 100 × 10 wing with side-edge separation and N_{sub} = 8. This solution was compared with that of the conventional Biot–Savart method, which used a similar discretization and no subvortices. There is reasonable agreement between the two computations. Once again, it can be seen that the VIC method provided higher loads throughout the span, especially at the tip. This problem is reduced as discretization is increased. Also shown in this plot are experimental data for section lift, from Ref. 17.

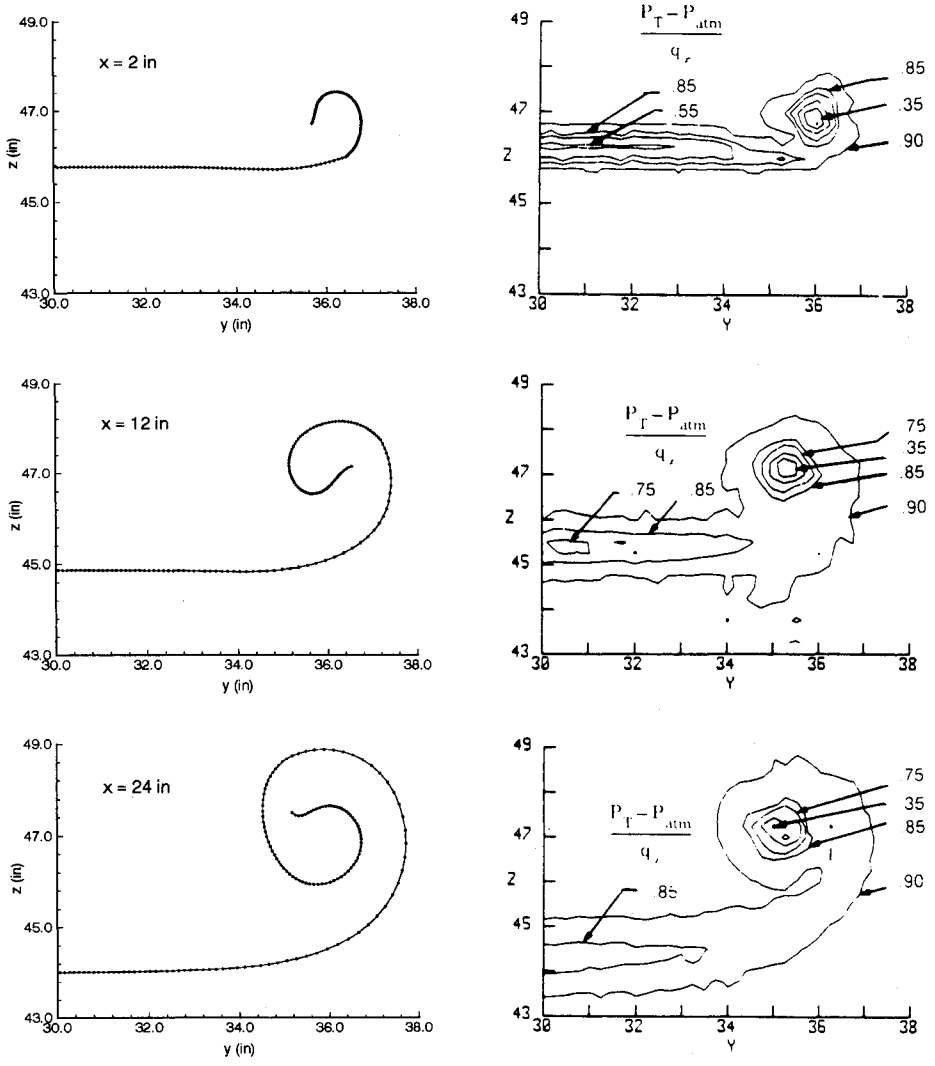

Fig. 8 Experimental contours of total pressure loss compared with computed wake position for three crossflow planes. Experimental data from Ref. 18. Rectangular wing, AR = 6.0, α = 8 deg.

The wake roll-up for an AR = 6.0 rectangular wing at α = 8 deg is described in Fig. 8. Wake shapes for three crossflow planes are compared with contours for total pressure loss obtained by Brune et al.[18] The wing chord length was 12 in. and the (y, z) coordinates refer to the 8 × 12 ft test section. The x coordinate has origin at the trailing edge. In the present calculation, the tip vorticity is highly concentrated in the last 10% of the vortices. The present method, which implemented side-edge separation, captured well the tip vortex in the proximity of the trailing edge. The vertical displacement and overall shape of the wake show very good agreement with the experimental results. The calculation used a 0.1 × 0.075 × 0.075 cell and 100 × 6 wing panels, and N_{sub} = 8.

Wake-Wing Close Interaction

El-Ramly et al.[19] performed wind-tunnel measurements for a two-wing, staggered configuration. The wing sizes simulated a commercial transport aircraft generating a wake that disturbed a small airplane. The experimental arrangement is sketched in Fig. 9. The upstream wing had AR = 7.0, taper ratio equal to 1/3, and was swept back 35 deg at the $c/4$ line. It was mounted along the test section centerline. The downstream wing had AR = 7.5 and was rectangular, with a span that was about 24% of the upstream wingspan. The smaller wing had no incidence, and was placed between 2.5–5 upstream-wingspans from its trailing edge.

The computation presented used a 0.225 × 0.1 × 0.1 cell, 25 × 3 panels for each half of the upstream wing and for the downstream wing, with no side-edge separation; N_{sub} = 8 and

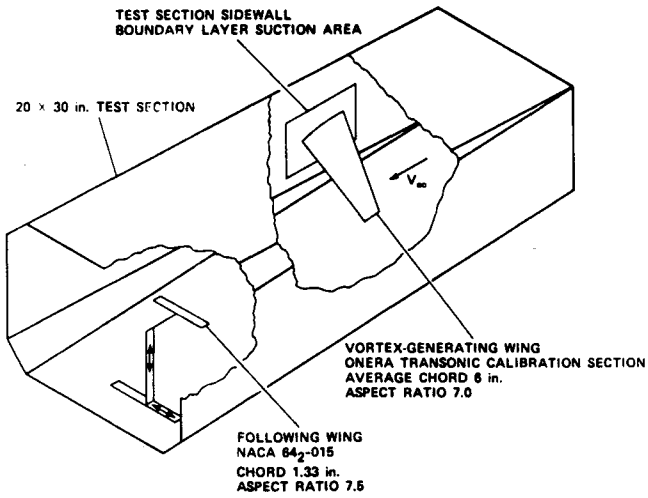

Fig. 9 Experimental arrangement for close interaction between tip vortex and wing, from El-Ramly et al.[19] (reproduced from Ref. 20).

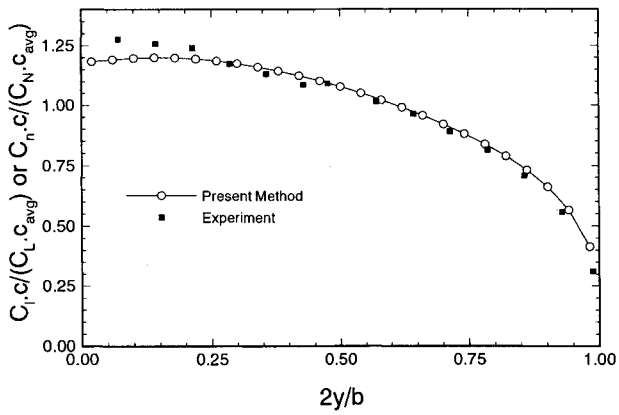

Fig. 10 Normalized load distribution for upstream wing at α = 5 deg. Present method results are for normal force. Experimental results[19] are for lift.

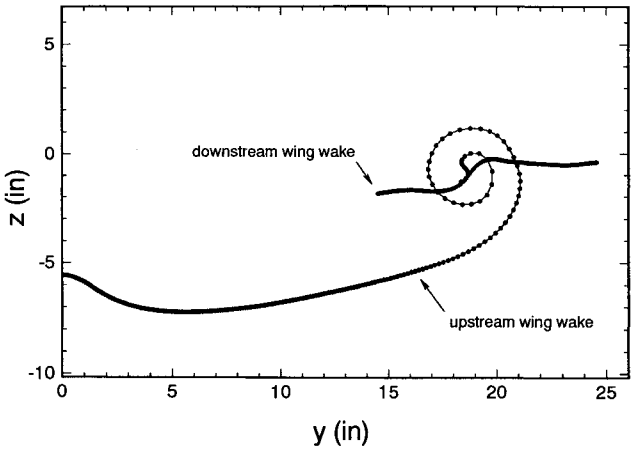

Fig. 11 Wake shapes at crossflow plane x = 5.8b, for the case of maximum rolling moment.

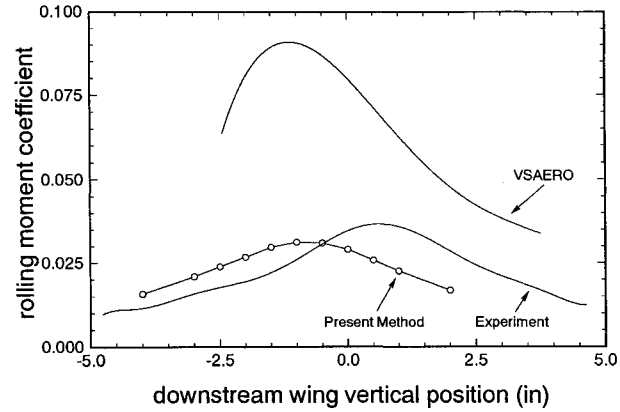

Fig. 12 Variation of rolling moment of the downstream wing with its vertical position. Results compared with experiment[19] and computations by VSAERO.[20]

X_{cutoff} = 5.8b, where b is the swept-wingspan, and the x origin is at the root trailing edge.

The normal force distribution along the span for the upstream wing is compared in Fig. 10 with the experimental data for lift at α = 5 deg, with very good agreement. The distributions are normalized by the total coefficients and the average chord c_{avg}. The differences at the root are due to errors in representing the "kink" in sweep with the vortex-lattice model.[2] The load decrease reverses the sign of the wake vortices at the root, which, although weak, produce a change in the wake geometry in that region, as seen in Fig. 11. This figure shows the rolled-up wake shapes at plane x = 5.8b. The downstream wing was 5.0b from the upstream one, and its root was 0.032b inboard of the upstream wingtip. Its vertical distance from the test section centerline was −1.0 in. Notice the smooth roll-up of the upstream wake, and the distortion of the downstream wake as both interact.

The rolling moments induced in the downstream wing are shown in Fig. 12, with upstream wing at α = 5 deg and downstream wing at the same 0.032b position. The present method results are compared with the experimental data and with computations from VSAERO.[20] There is a shift between the computed and experimental curves due to different vertical positions of the upstream tip vorticity. This is partly due to interference from the tunnel wall, which is only 0.42b from the upstream wingtip, creating a strong image vortex. Other than that, the shape and peak value obtained with the present method agree very well with the experimental results. No special care had to be exercised when the tip vorticity impinged directly on the downstream wing, and the discretiza-

tion was kept the same. The results from VSAERO, which is a low-order panel method that allows wing relaxation, overpredicted the rolling moment by a large margin.

Next, the geometry in Ref. 21 was analyzed (see Fig. 13). It consisted of two wings in a cruciform arrangement. The generating wing was placed at $\alpha = 12.6$ deg. The leading edge of the following wing was placed at two generating chords c_g from the trailing edge of the generating wing, and had no incidence. Notice the difference in chord size between the two wings. The position of the following wing was specified relative to the position of the tip vortex of the upstream wake for the generating wing alone. When the tip vortex position at $2c_g$ behind the generating wing was determined, the following wing was placed so that the vortex was at 25% of its span. The vortex vertical displacement z_v was given as a fraction of the following wing chord c_f and was positive above the wing.

The orientation of the wings was changed for the computations, placing the generating wing parallel to y and the following wing in the vertical position. The present method used a $0.085 \times 0.075 \times 0.075$ cell size, 100×6 panels for the upstream wing (side separation present), 60×6 for the downstream one, $N_{sub} = 8$ and $X_{cutoff} = 4.25c_g$. The origin for x is at the upstream wing trailing edge.

Figures 14 and 15 present the computed section normal force distribution, compared with the experimental data and with results from VSAERO.[20] In the VSAERO computations, a small number of iterations for the relaxation procedure was applied, and only for the upstream wake. The cases

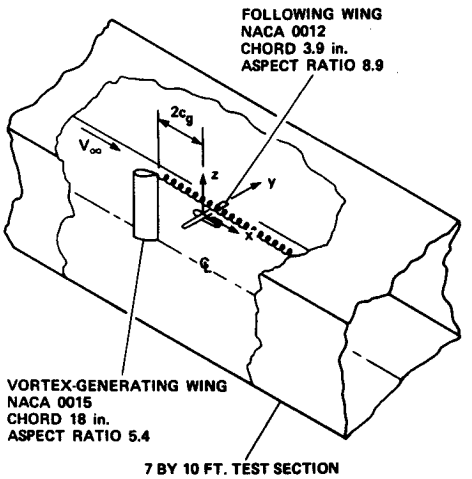

Fig. 13 Experimental arrangement for close interaction between tip vortex and wing, from McMillan et al.[21] (reproduced from Ref. 20).

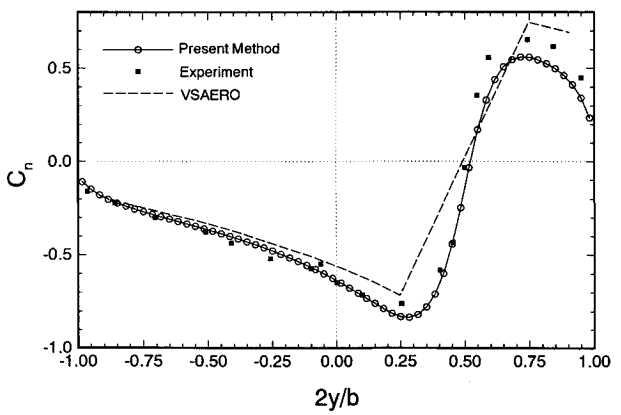

Fig. 14 Section normal force distribution for following wing at position $z_v/c_g = -0.02$. Results compared to those from experiment[21] and VSAERO.[20]

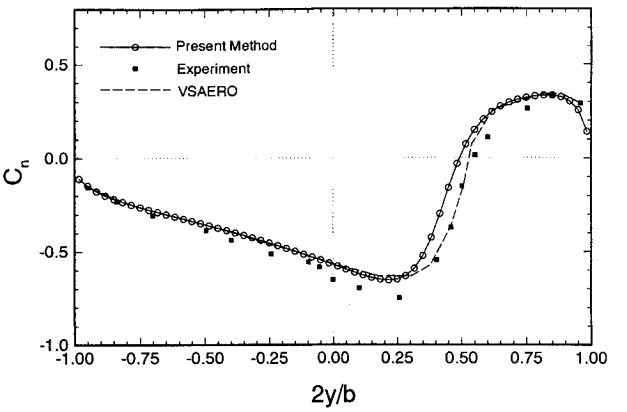

Fig. 15 Same as Fig. 14, for $z_v/c_g = 0.73$.

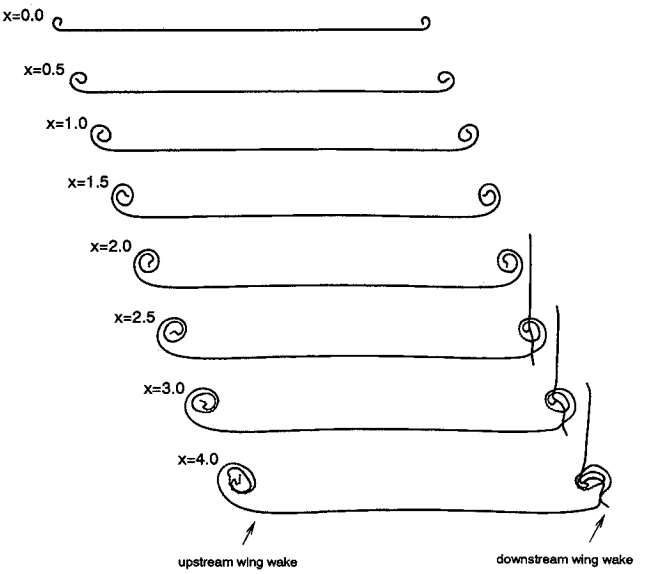

Fig. 16 Wake shapes at various crossflow planes for following wing at $z_v/c_g = -0.02$.

with strong wake-wing interaction would sometimes present instabilities, even after careful discretization to avoid vortex-panel proximity. For the present computations, it can be seen that the results agree very well with the experiment. As in the previous case, no special care was needed regarding discretization for close interaction cases, although the discretization was very fine. Rolled-up wake shapes at various crossflow planes for the case of $z_v/c_g = -0.02$ are shown in Fig. 16. For this computation, the relaxation step was executed 90 times (for tolerance of $0.01c_g$) and the circulation correction 53 times (for a tolerance of 0.5%), using a $65 \times 129 \times 33$ grid.

Conclusions and Comments

A hybrid method composed of a VIC formulation for velocity computation and a vortex-lattice model for wings was applied with success to several one- and two-wing configurations. The VIC method uses an infinite domain fast Poisson solver and a subvortex technique. This technique allows an increase in the wake discretization without change in the number of surface panels. The method performs best when wing panel and grid-cell dimensions are comparable, so that the grid truly represents vorticity layers. Normal forces and wake shapes for single wings presented good agreement with experiments and other calculations, although side-edge separation required fine discretizations to produce accurate load values. Forces and rolling moments induced on wings by upstream wakes were computed with good experimental agree-

ment, without special concern over discretization for cases with strong interaction.

Acknowledgments

This work was supported by a grant from CNPq (Conselho Nacional de Desenvolvimento Científico e Tecnológico, Brasília, Brazil) and Embraer S.A., who jointly sponsored the first author's Ph.D. studies at Stanford University.

References

[1]Maskew, B., "Predicting Aerodynamic Characteristics of Vortical Flows on Three-Dimensional Configurations Using a Surface-Singularity Panel Method," AGARD CP-342, 1983.

[2]Katz, J., and Plotkin, A., *Low-Speed Aerodynamics—From Wing Theory to Panel Methods*, McGraw–Hill, New York, 1991.

[3]Christiansen, J. P., "Numerical Simulation of Hydrodynamics by the Method of Point Vortices," *Journal of Computational Physics*, Vol. 13, 1973, pp. 363–379.

[4]Baker, G. R., "The 'Cloud-in-Cell' Technique Applied to the Roll Up of Vortex Sheets," *Journal of Computational Physics*, Vol. 31, 1979, pp. 76–95.

[5]Coüet, B., Buneman, O., and Leonard, A., "Simulation of Three-Dimensional Incompressible Flows with a Vortex-in-Cell Method," *Journal of Computational Physics*, Vol. 39, 1981, pp. 305–328.

[6]Coüet, B., and Leonard, A., "Exact Extension to the Infinite Domain for the Vortex-in-Cell Method," *SIAM Journal of Scientific and Statistical Computing*, Vol. 2, No. 3, 1981, pp. 311–320.

[7]Ribeiro, R., and Kroo, I., "Wake Roll-Up Analysis Using a Three-Dimensional Vortex-in-Cell Method," AIAA Paper 91-3312, Sept. 1991.

[8]Karamcheti, K., *Principles of Ideal-Fluid Aerodynamics*, Krieger, Malabar, FL, 1980.

[9]Ribeiro, R. S., "Analysis of Wing Wake Roll-Up Using a Vortex-in-Cell Method," Ph.D. Dissertation, Stanford Univ., Stanford, CA, 1992.

[10]James, R. A., "The Solution of Poisson's Equation for Isolated Source Distributions," *Journal of Computational Physics*, Vol. 25, 1977, pp. 71–93.

[11]Mittelman, Z., "Prediction of Unsteady Aerodynamics and Control of Delta Wings with Tangential Leading Edge Blowing," Ph.D. Dissertation, Stanford Univ., Stanford, CA, 1989.

[12]Schlichting, H., and Truckenbrodt, E., *Aerodynamics of the Airplane*, McGraw–Hill, New York, 1979.

[13]Maskew, B., "Subvortex Technique for the Close Approach to a Discretized Vortex Sheet," *Journal of Aircraft*, Vol. 14, No. 2, 1977, pp. 188–193.

[14]Krasny, R., "Computation of Vortex Sheet Roll-Up," *Lecture Notes on Mathematics 1360*, Springer–Verlag, Berlin, 1988.

[15]Von Scholz, N., "Kraft und Druckverteilungsmessungen an Tragflachen Kleiner Streckung," *Forscharb. Ing. Wes.*, No. 16, 1949, pp. 85–92.

[16]Yeh, D. T., and Plotkin, A., "Vortex Panel Calculation of Wake Rollup Behind a Large Aspect Ratio Wing," AIAA Paper 85-1561, July 1985.

[17]McAlister, K. W., and Takahashi, R. K., "NACA 0015 Wing Pressure and Trailing Vortex Measurements," NASA TP-3151, Aug. 1991; also USAAVSCOM TR-91-A-003, March 1991.

[18]Brune, G. W., and Bogataj, P. W., "Induced Drag of a Simple Wing from Wake Measurements," Society of Automotive Engineers TP 901934, Oct. 1990.

[19]El-Ramly, Z., Rainbird, W. J., and Earl, D. G., "Wind Tunnel Measurements of Rolling-Moment in a Swept-Wing Vortex Wake," *Journal of Aircraft*, Vol. 13, No. 12, 1976, pp. 962–967.

[20]Smith, B. E., and Ross, J. C., "Application of a Panel Method to Wake Vortex/Wing Interaction and Comparison with Experiment," AIAA Paper 84-2182, Aug. 1984.

[21]McMillan, O. J., Schwind, R. G., and Nielsen, J. N., "Rolling Moments in a Trailing Vortex Flow Field," NASA CR-151961, 1977.